

GNSS Satellite Orbit and Clock Truth Generation for ARAIM Offline Monitoring

Jaymin Patel, *Illinois Institute of Technology*
Samer Khanafseh, *Illinois Institute of Technology*
Boris Pervan, *Illinois Institute of Technology*

BIOGRAPHY

Jaymin Patel is a Ph.D. student at Navigation Laboratory in the Department of Mechanical and Aerospace Engineering at IIT. He received his B.S. in Mechatronics Engineering from Ganpat University, Gujarat, India and M.E degree in Mechanical and Aerospace Engineering, from the IIT. His research interest includes the design of high accuracy and high integrity navigation algorithms, fault detection for Ground Based Augmentation Systems (GBAS) and fault monitoring for Advanced Receiver Autonomous Integrity Monitoring (ARAIM). He was the recipient of the Best Student Paper Award in the 2018 IEEE/ION PLANS conference.

Dr. Samer Khanafseh is currently a research assistant professor at Illinois Institute of Technology (IIT), Chicago. He received his MSc and PhD degrees in Aerospace Engineering from IIT in 2003 and 2008, respectively. Dr. Khanafseh has been involved in several aviation applications such as Autonomous Airborne Refueling (AAR) of unmanned air vehicles, autonomous shipboard landing for NUCAS and JPALS programs and Ground Based Augmentation System (GBAS). His research interests are focused on high accuracy and high integrity navigation algorithms, cycle ambiguity resolution, high integrity applications, fault monitoring and robust estimation techniques. He was the recipient of the 2011 Institute of Navigation Early Achievement Award for his outstanding contributions to the integrity of carrier phase navigation systems.

Dr. Boris Pervan is a Professor of Mechanical and Aerospace Engineering at IIT, where he conducts research on advanced navigation systems. Prior to joining the faculty at IIT, he was a spacecraft mission analyst at Hughes Aircraft Company (now Boeing) and a postdoctoral research associate at Stanford University. Prof. Pervan received his B.S. from the University of Notre Dame, M.S. from the California Institute of Technology, and Ph.D. from Stanford University. He is an Associate Fellow of the AIAA, a Fellow of the Institute of Navigation (ION), and Editor-in-Chief of the ION journal NAVIGATION. He was the recipient of the IIT Sigma Xi Excellence in University Research Award (2011, 2002), Ralph Barnett Mechanical and Aerospace Dept. Outstanding Teaching Award (2009, 2002), Mechanical and Aerospace Dept. Excellence in Research Award (2007), University Excellence in Teaching Award (2005), IEEE Aerospace and Electronic Systems Society M. Barry Carlton Award (1999), RTCA William E. Jackson Award (1996), Guggenheim Fellowship (Caltech 1987), and Albert J. Zahm Prize in Aeronautics (Notre Dame 1986).

ABSTRACT

This paper describes the generation of “truth” satellite orbit and clock product for advanced receiver autonomous integrity monitoring (ARAIM) offline monitor. The ARAIM user algorithm, which includes fault detection and exclusion (FDE), is autonomously executed at the airborne receiver. To achieve specific integrity and continuity requirements, the real-time FDE process requires assertions on the signal-in-space (SIS) performance, in particular on satellite clock and orbit ephemeris error characteristics. This information is broadcast in the integrity support message (ISM). The offline ground monitor estimates precise GNSS satellite orbits and clocks which are utilized to validate the ISM. In contrast to other sophisticated orbit determination processes that focus on accuracy for performance, such as the one used by the international GNSS service (IGS), the proposed offline monitor (OFM) architecture is mainly intended for safety-critical aviation applications, in which integrity is of primary concern. This monitor employs a straightforward approach to estimate satellite orbit/clock using the existing satellite based augmentation system (SBAS) ground infrastructure. For prototyping purpose, twenty sparsely-distributed reference stations (RS) are selected from a worldwide network of IGS stations, and their publicly-available observation data is utilized. A parametric satellite orbital model is employed in the estimator, whose implementation is described in the paper. Initially, the GPS legacy orbit model is utilized to analyze the impact of different error sources on the estimation and to resolve

numerical issues on the estimator. And we show that signal-in-space ranging error due to our product of satellite orbit and clocks are in the order of decimeter.

I INTRODUCTION

The main challenge when using global navigation satellite systems (GNSS) in safety-critical civil aviation application is to mitigate the integrity threats caused by measurement faults, including satellite and constellation failures [1]. For the single constellation (GPS), receiver autonomous integrity monitoring (RAIM) utilize for fault detection as a backup navigation tool to support aircraft en-route flight [2]–[4]. The core principle of RAIM is to exploit redundant measurements to achieve self-contained FD at the user receiver [5].

With the modernization of GPS (U.S.), the full deployment of GLONASS (Russia), Galileo (European Union) and Beidou (China) [6], the number of redundant ranging signals increases dramatically, which opens the possibility to independently support worldwide aircraft navigation. This includes supporting stringent requirements for vertical guidance of aircraft down to 200 feet altitude above the runway [7]–[9]. Most importantly, by taking advantages of the revolutionary developments in GNSS, the reliance on the ground infrastructure will be alleviated in future ARAIM. Therefore researchers in the European Union and in the United States [10], [11], are developing new dual-frequency, multi-constellation ARAIM fault detection and exclusion (FDE) methods.

To incorporate information from multiple constellations at different stages of their development, ARAIM relies on Integrity Support Messages (ISM) which is generated using offline monitor (OFM) and broadcast to airborne receivers. The ISM provides integrity parameters describing measurement errors and faults such as for example, the prior probability of satellite faults, the prior probability of constellation-wide faults, and the standard deviation of nominal ranging measurement uncertainty due to satellite orbit and clock ephemeris errors [7], [8]. These integrity parameters are vital inputs to the airborne ARAIM algorithm, which defines positioning error bounds called protection levels (PL). In current conventional RAIM implementations, these integrity parameters are defined by the GPS constellation service provider (CSP) commitments and are hard-coded in the receiver. For ARAIM implementations, the ISM parameters will be generated and validated at the ground, and updated to users as needed. Various methods of ISM dissemination are presently being considered, including broadcast on the CSP navigation message. The methods and results described in this paper are applicable regardless of the way of dissemination.

To validate the ISM, ‘online’ and ‘offline’ ARAIM architectures have been investigated [8], [12]. Offline architectures have generally been perceived as preferable because they do not require frequent communication between users and ground segment, thereby eliminates the connectivity risk [8]. An offline ARAIM monitor would rely on post-processed GNSS measurements, collected from twenty ground stations, to bound errors in the CSP broadcast navigation messages on a long-term basis. To do this, prior research utilized truth satellite positions and clock biases from the international GNSS service (IGS) network [13]–[15]. However, given that ARAIM is intended to operate over several decades, monitor dependence on external organizations with little or no stake in civil aviation must be carefully considered, and ideally, avoided. Most importantly, ARAIM will be used in safety-critical applications. All potential sources of a safety risk, including the monitor’s truth data, must be appropriately accounted. The IGS, the national geospatial intelligence agency (NGA), and others currently provide high-accuracy satellite orbit and clock products. However, none of these agencies make specific commitments on the reliability of their products, or on the processes used to obtain those products. Further, data gaps exist in those products, especially during satellite fault events, which are crucial to ARAIM. In response, this paper provides a new approach to produce satellite orbit and clock product using a dedicated ARAIM OFM. The estimated satellite orbit and clocks can then be differenced from the GNSS broadcast navigation message to determine satellite orbit and clock errors. This satellite orbit/clock error data would provide the means to validate the ISM parameters.

There has been prior work to analyze a dedicated ARAIM OFM [16]. The monitor employs a transparent and straightforward orbit determination process, intended to facilitate integrity analysis. The process is based on well-established parametric orbit models for medium-earth-orbiting satellites, which are accurate for up to four-hour time intervals. The fidelity of the orbit model was validated by quantifying residual errors relative to known satellite positions [16]. Also, the monitor may utilize existing global SBAS ground infrastructure. Twenty SBAS reference stations (RS) are considered to continuously estimate satellite positions and clock biases. In [16], covariance analysis was carried out to assess the impact of RS measurement uncertainty on satellite position and clock estimation. It indicated that the standard deviation of the monitor’s estimated orbit/clock error should be on the order of 30 cm. In a preliminary prototype, we have developed the code error model for the receiver site and analyzed its impact on the estimator [17]. The preliminary result showed that the estimated satellite orbit and clocks errors are in the order of meters.

In this paper, we continue a prototype to reduce estimated error from meter to decimeter level. Since we expect the pretty low estimated error, we need to analyze the estimator carefully. In the following sections, the paper discusses the required OFM performance, the OFM architecture, the proposed estimator design and result using GPS legacy model.

II REQUIRED OFM PERFORMANCE

Using an OFM, the update rate of the ISM may vary from a month to multiple years depending on variations in constellation performance [8]. A large amount of data will be processed at the ground to obtain the ISM, which is expected to bound the signal-in-space (SIS) performance until the next update. To achieve this, differences between broadcast ephemeris and the monitor's estimated satellite orbit/clock will be first evaluated over time, and then these will be used to validate (or modify, if needed) the ISM parameter values. In this paper, we mainly focus on producing satellite orbit and clock estimates to validate b_{nom} and σ_{URA} , which specify a Gaussian bound on the SIS performance under nominal conditions, (i.e., no faults). Since the monitor's orbit/clock estimation errors will directly contribute to our ability to validate ISM, it is necessary to first define the required accuracy of the monitor's orbit/clock estimator.

Equation (1) shows the relationship between the actual standard deviations of broadcast satellite orbit/clock error σ_{URA} , the standard deviation of the monitor's estimated orbit/clock error σ_{OFM} , and the validated standard deviation of the satellite orbit/clock error $\alpha \sigma_{URA}$ (validated σ_{URA}). (In the ISM, the multiplying factor, α , is updated rather than $\alpha \sigma_{URA}$).

$$\alpha \sigma_{URA} = \sqrt{\sigma_{URA}^2 + \sigma_{OFM}^2} \quad (1)$$

Figure 1 shows $\alpha \sigma_{URA}$ vs σ_{OFM} for an example broadcast σ_{URA} value of 1 m. According to the most recent study on GPS SIS performance to support ARAIM, the maximum σ_{URA} of 1 m, or less is observed on space vehicle number (SVN) 61. Moreover, dual-constellation ARAIM availability simulations have revealed localizer performance with vertical guidance (LPV)-200 approach can only be supported when σ_{URA} of both constellations are approximately 1 m [8]. The Figure shows the slow growth of $\alpha \sigma_{URA}$ as σ_{OFM} increases. Even when σ_{OFM} reaches 0.5 m, i.e., half of σ_{URA} , the achievable validated σ_{URA} is still around 1.12 m.

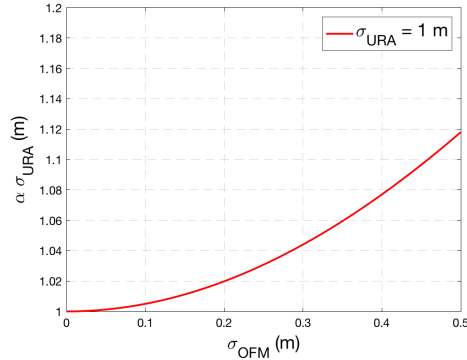


Fig. 1. Sensitivity of OFM on validating σ_{URA}

In addition to σ_{OFM} , the estimated satellite orbit/clock error may have a non-zero mean, denoted by b_{OFM} . This term is accounted as one component of the validated ISM parameter, b_{nom} . However, using baseline solution separation ARAIM user algorithm [10], the absolute value of b_{nom} is additive for each measurement. This causes the integrity risk bound to become loose as the number of measurements increases, thereby degrading availability performance [10]. Therefore, it is desirable to mitigate any contributions of b_{OFM} to the validated b_{nom} .

From the previous discussion, it can be seen that the required accuracy of the offline monitor is significantly lower than the precise satellite orbit/clock products by IGS or NGA. Instead, it is the reliability of the monitor's estimator output that is key. In other words, even though the monitor's satellite orbit/clock estimates may have larger errors most of the time, their stable performance and consistent availability will enable ISM validation without data gaps, especially at crucial times when SV

faults occur. Therefore, it is not necessary to pursue a complicated orbit determination process. Instead, a transparent approach is described to estimate satellite orbit and clock biases in the next section.

III ARCHITECTURE OF THE OFM PROTOTYPE

This section describes the OFM architecture step-by-step. A network of worldwide sparsely distributed RS is employed to collect code and carrier measurements over time. In the selection of sites for the RS, we take advantage of the SBAS ground infrastructures since they are already installed and designed to support civil aviation applications. Figure 2 shows all existing SBAS RS across the globe. For the prototype, we have selected 20 RS shown in Figure 3. Because SBAS data are not publicly accessible, we use RS from the IGS network as a surrogate for SBAS RS. This network ensures that each satellite can continuously be tracked by at least 3 RS (Fewer than 3 RS could degrade the monitoring performance).

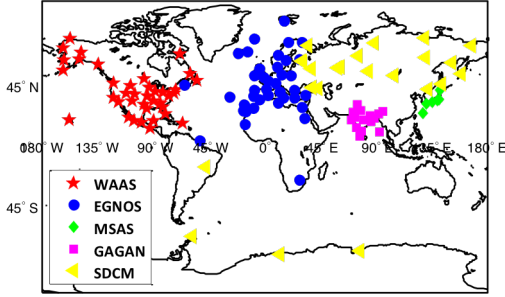


Fig. 2. ALL existing SBAS stations

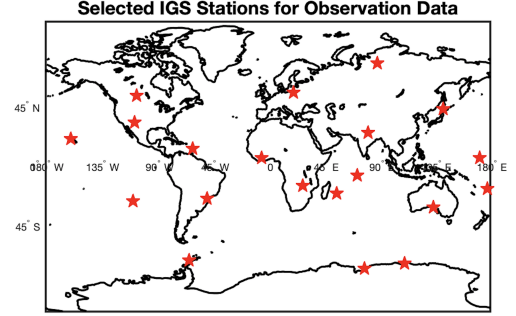


Fig. 3. Selected IGS stations for the prototype

The OFM uses parametric orbit models to determine space vehicle (SV) trajectories. From prior work, it is known that the 17-parameter CNAV model outperforms the 15-parameter GPS legacy model [16]. However, in this paper, we show the methodology to generate precise product using GPS legacy model only. Moreover, the prototype assumes no satellite maneuvers occur because the orbit models would not be valid. Since maneuvers occur rarely, and they can be handled in post-processing by simply initiating a new estimator after the maneuver. The OFM estimates orbit model parameters, SV clock biases and RS clock biases assuming no satellite maneuver.

Let p_i^{orb} be a 15 x 1 vector of orbit parameters for SV i , and let g_k^{orb} be the non-linear function that determines SV orbit. The true SV position X_k^i of SV i at time epoch k can be expressed as:

$$X_k^i = g_k^{orb}(p_i^{orb}) + v_k^{orb,i} \quad (2)$$

where $v_k^{orb,i}$ is the deviation of model output from the actual position X_k^i . $v_k^{orb,i}$ represents the model's inability to capture the exact orbit. These model fidelity errors can be bounded by a zero-mean Gaussian distribution with a standard deviation of 12 cm [16]. The GPS orbit model is valid over a four-to-six hour time interval noted T_{FIT} [18]. Sensitivity to T_{FIT} has been evaluated in our prior work in [19]. We use a four-hour fitting interval, which is the most common value for GPS ephemeris.

Both RS and SV are equipped with atomic clocks, and a quadratic polynomial can be employed to model their nominal errors. However, most SV faults are caused by their clocks, and for the monitor to observe them, no assumption can be made on the SV clock dynamics. As for the RS clocks, covariance analysis indicated that the performance of OFM is not improved much with a quadratic model on RS clock errors [16]. Thus, no assumption is made on RS clocks.

The ionospheric-free code and carrier phase measurements (dual-frequency) for SV i from RS j at time epoch k are expressed in the following two equations:

$$\rho_k^{i,j} = \|X_j - X_{i,k}\| - \tau_{i,k} + b_{j,k} + c(d_j + d^i) + T_k^{i,j} + \mathcal{E}_{RNM,\rho,k}^{i,j} \quad (3)$$

$$\phi_k^{i,j} = \|X_j - X_{i,k}\| - \tau_{i,k} + b_{j,k} + c(\delta_j + \delta^i) + \eta^{i,j} + T_k^{i,j} + \mathcal{E}_{RNM,\phi,k}^{i,j} \quad (4)$$

Where,

X_j : known antenna location of RS j after applying solid earth tide correction (Appendix B for details)

$X_{i,k}$: unknown antenna phase center location of SV i at time k
 $\tau_{i,k}$: unknown clock offset of SV i at time k
 $b_{j,k}$: unknown clock offset of RS j at time k
 d^i, d_j : instrumental delay in the receiver j and satellite i for L1/L2 code phase measurements
 δ^i, δ_j : instrumental delay in the receiver j and satellite i for L1/L2 carrier phase measurements
 $\eta^{i,j}$: unknown, constant iono-free carrier phase cycle ambiguity for SV i at RS j
 $\| \cdot \|$: Euclidean norm operator, in this case providing the distance between RS j and SV i
 $T_k^{i,j}$: Tropospheric delay errors for SV i and RS j at time k

The receiver noise and multipath (RNM) errors are denoted by $\varepsilon_{RNM,\rho,k}^{i,j}$ and $\varepsilon_{RNM,\phi,k}^{i,j}$ for code and carrier respectively. The error models for RNM are described later in Section VI. Although the ARAIM OFM will utilize L1 and L5 frequencies to generate a precise product, the prototype demonstrates the methodology using L1 and L2 frequencies.

The satellite instrumental delay changes slowly over a day on the order of a millimeter. Since our expected performance is at the level of decimeters, we assume the satellite instrumental delay to be constant over a day [25]. An individual instrumental delay is not observable, but differential delay between two frequencies or types of pseudorange measurements is observable. For example, the L1 C/A signal experiences delay related to the ionosphere-free satellite clock, which is corrected using the timing group delay (TGD). In general, a Differential Code Bias (DCB) is defined as the difference between two instrumental delays. Depending on the type of measurements, DCB correction is applied (Appendix A). The satellite DCB correction is crucial as it would behave like a constant SV clock bias if not needed. On the other hand, the exact RS clock bias is not desired. So, it is not necessary to correct the receiver instrument delay. Similar to the code instrumental delay, carrier phase also experiences a constant instrumental delay that would be estimated with the cycle ambiguities.

The range term in equations (3) and (4) represents the precise distance between the satellite antenna phase center (APC) and receiver APC. To estimate the precise SV position, we also need to calibrate APC for each RS and each frequency. Since we are using IGS RS sites, APC calibration is directly available for L1 and L2 frequencies as solution independent exchange (SINEX) format [27]. The following equation shows the deviation of the known antenna location to APC.

$$\delta r_{APC} = \frac{f_{L1}^2}{f_{L1}^2 - f_{L2}^2} \delta r_{L1} - \frac{f_{L2}^2}{f_{L1}^2 - f_{L2}^2} \delta r_{L2} \quad (5)$$

Where,

δr_{L1} : calibrated vector between antenna to APC of L1 frequency
 δr_{L2} : calibrated vector between antenna to APC of L2 frequency
 δr_{APC} : resultant APC correction vector

To correct for tropospheric delay effect, we have considered the Neutral Atmosphere Model, developed by the University of New Brunswick, Fredericton, Canada (UNB3m) [21]. They show that the residuals of the UNB3m model are approximately zero mean with a standard deviation of 5 cm observed throughout 7 years of data. In this work, we model these residual errors as a function of zenith tropospheric delay (ZTD) using a mapping function (c_T) given in [8], [10], [11].

$$T_k^{i,j} = T_{i,j,k}^{model} + c_T \varepsilon_{tropo,j}^{ZTD} \quad (6)$$

To estimate the SV orbit parameters and clocks, the measurement equations (3) and (4) and the orbit model equation (2) are linearized and incorporated into a single filter. We illustrate this process for code measurements in the following derivation. Using broadcast ephemeris ($X_{i,k}^*$) and the tropo correction in equation (6):

$$\begin{aligned} \delta \rho_k^{i,j} &= \rho_k^{i,j} - \|X_j - X_{i,k}^*\| - T_{i,j,k}^{model} - c \frac{f_{L1}^2}{f_{L1}^2 - f_{L2}^2} DCB_{C1C-C1W}^i + {}^{i,j}e_k^T \delta r_{APC,j,k} \\ &= {}^{i,j}e_k^T \delta X_{i,k} - \tau_{i,k} + b_{j,k} + c_T \varepsilon_{tropo,j}^{ZTD} + \varepsilon_{RNM,\rho,k}^{i,j} \end{aligned} \quad (7)$$

Where,

δ : deviation from nominal values, i.e $\delta X_{i,k} = X_{i,k} - X_{i,k}^*$
 ${}^{i,j}e_k$: 3 x 1 line of sight (LOS) unit vector from RS j to SV i at time k

In the next step, the orbit model is linearized at $*p_i^{orb}$ where, $X_{i,k}^* = g_k^{orb}(*p_i^{orb})$. Substituting the linearized orbit model equation into the code measurement, equation (7) becomes:

$$\delta \rho_k^{i,j} = {}^{i,j}e_k^T A_{i,k}^{orb} \delta p_{i,k}^{orb} - \tau_{i,k} + b_{j,k} + c_T \varepsilon_{tropo,j}^{ZTD} + \varepsilon_{RNM,\rho,k}^{i,j} \quad (8)$$

Where,

$A_{i,k}^{orb}$: Jacobian matrix for the SV orbit model in equation (2), which is 3 x 15 for the GPS legacy orbit model. It is composed of numerically-derived partial derivatives of the position coordinates of SV i at time k , $X_{i,k} = [x_{i,k} \quad y_{i,k} \quad z_{i,k}]^T$ with respect to the orbit parameters $p_i^{orb} = [p_1 \quad \dots \quad p_{15}]^T$

$$A_{i,k}^{orb} = \begin{bmatrix} \frac{\partial x_{i,k}}{\partial p_1} & \dots & \frac{\partial x_{i,k}}{\partial p_{15}} \\ \frac{\partial y_{i,k}}{\partial p_1} & \dots & \frac{\partial y_{i,k}}{\partial p_{15}} \\ \frac{\partial z_{i,k}}{\partial p_1} & \dots & \frac{\partial z_{i,k}}{\partial p_{15}} \end{bmatrix}_{3 \times 15} \quad (9)$$

We define the product of line-of-sight vector and Jacobian matrix as,

$$B_k^{i,j} \triangleq i,j e_k^T A_{i,k}^{orb} \quad (10)$$

Equation (8) is timetagged using internal receiver clock, which may not be synced between all RS used. While considering multiple RS in the estimator, a time-alignment correction term is necessary to achieve sub-meter level precision [17]. This correction modifies the receiver clock bias term as shown in equation (11).

$$\begin{aligned} \delta \rho_k^{i,j} &= B_k^{i,j} \delta p_{i,k}^{orb} - \tau_{i,k} + \frac{c - \dot{\phi}_k}{c} b_{j,k} + c_T \varepsilon_{tropo,j}^{ZTD} + \varepsilon_{RNM,\rho,k}^{i,j} \\ &= B_k^{i,j} \delta p_{i,k}^{orb} - \tau_{i,k} + \varphi_k b_{j,k} + c_T \varepsilon_{tropo,j}^{ZTD} + \varepsilon_{RNM,\rho,k}^{i,j} \end{aligned} \quad (11)$$

Where, φ_k is defined as $\varphi_k = \frac{c - \dot{\phi}_k}{c}$, c is the speed of light and $\dot{\phi}$ is the SV doppler rate

Similarly, the linearized carrier phase measurement can be written as,

$$\delta \phi_k^{i,j} = B_k^{i,j} \delta p_{i,k}^{orb} - \tau_{i,k} + \varphi_k b_{j,k} + \eta^{i,j} + c_T \varepsilon_{tropo,j}^{ZTD} + \varepsilon_{RNM,\phi,k}^{i,j} \quad (12)$$

IV ESTIMATOR DESIGN

The designed estimator utilizes equations (11) and (12) as measurements. The parameters to be estimated or ‘states’ include SV orbit parameters δp_i^{orb} , SV clock $\tau_{i,k}$, RS clock $b_{j,k}$, cycle ambiguities $\eta^{i,j}$ and zenith tropospheric delay residual $\varepsilon_{tropo,j}^{ZTD}$. An information smoother is implemented to estimate these states over T_{FIT} of 4 hours simultaneously. A sample period of 4 minutes is selected assuming that, at such infrequent intervals, measurement error correlation due to RS multipath would be negligible.

Measurement model

$$\begin{bmatrix} \delta \rho^{1,1} \\ \delta \rho^{1,2} \\ \vdots \\ \delta \rho^{1,20} \\ \delta \rho^{2,1} \\ \vdots \\ \delta \rho^{32,20} \\ \delta \phi^{1,1} \\ \vdots \\ \delta \phi^{32,20} \end{bmatrix}_k = \begin{bmatrix} B^{1,1} & \dots & 0 & -1 & \dots & 0 & 0 & \dots & 0 & 0 & \dots & 0 & c_T & \dots & 0 \\ B^{1,2} & \dots & 0 & -1 & \dots & 0 & 1 & \dots & 0 & 0 & \dots & 0 & 0 & c_T & \dots & 0 \\ \vdots & & \vdots & \vdots & \dots & \vdots & \vdots & \dots & \vdots & \vdots & \dots & \vdots & \vdots & \dots & \vdots \\ B^{1,20} & \dots & 0 & -1 & \dots & 0 & 0 & \dots & 1 & 0 & \dots & 0 & 0 & \dots & c_T \\ 0 & B^{2,1} & \dots & 0 & 0 & -1 & \dots & 0 & 0 & \dots & 0 & 0 & c_T & 0 & \dots & 0 \\ \vdots & & \ddots & \vdots & & \ddots & \vdots & & \vdots & & \ddots & \vdots & & & & \\ 0 & \dots & & B^{32,20} & 0 & & -1 & 0 & \dots & 1 & 0 & \dots & 0 & & & c_T \\ B^{1,1} & \dots & 0 & -1 & \dots & 0 & 0 & \dots & 0 & 1 & \dots & 0 & c_T & \dots & & 0 \\ \vdots & & \vdots & \vdots & \dots & \vdots & \vdots & \dots & \vdots & \vdots & \dots & \vdots & \vdots & \dots & \vdots \\ 0 & \dots & & B^{32,20} & 0 & \dots & -1 & 0 & \dots & 1 & 0 & \dots & 1 & 0 & \dots & c_T \end{bmatrix}_k \begin{bmatrix} \delta p_1^{orb} \\ \vdots \\ \delta p_{32}^{orb} \\ \tau_1 \\ \vdots \\ \tau_{32} \\ b_2^{c1k} \\ \vdots \\ b_{20}^{c1k} \\ \eta^{1,1} \\ \vdots \\ \eta^{32,20} \\ \varepsilon_{tropo,1}^{ZTD} \\ \vdots \\ \varepsilon_{tropo,20}^{ZTD} \end{bmatrix}_k + \begin{bmatrix} \varepsilon_{\rho}^{1,1} \\ \varepsilon_{\rho}^{1,2} \\ \vdots \\ \varepsilon_{\rho}^{1,20} \\ \varepsilon_{\rho}^{2,1} \\ \vdots \\ \varepsilon_{\rho}^{32,20} \\ \varepsilon_{\phi}^{1,1} \\ \vdots \\ \varepsilon_{\phi}^{32,20} \end{bmatrix}_k \quad (13)$$

For time epoch k , code and carrier measurements are collected from RS 1 to 20 for all PRN (SV) 1 to 32 and stacked in a linearized measurement vector in equation (13). Estimator states are grouped and identified using different colors: green for orbit parameter, yellow for SV clock bias, gray for RS clock bias, blue for ambiguities and orange for zenith tropospheric delay (ZTD) residual. The first and second superscript represents SV and RS respectively. Since measurements are written for time epoch k , all terms are scalar except the orbit parameter terms (δP_i^{orb}): 15×1 and $B^{i,j}$: 1×15 (for the legacy model). There is one important aspect to point out; the determination of the satellite and receiver clock bias can only be made in a differential way, so a time reference must be implicitly established. In the framework of this prototype, RS 1 clock is considered as the reference. Thus, b_1^{clk} state is not included in the state vector of equation (13).

Due to singularities in the orbit model, the estimator can experience numerical issues. For example, a circular satellite orbit where eccentricity (e) is zero causes the line of apsis and the argument of perigee (ω) to be undefined. In prior work, we have replaced ω, e, M_0 parameters with nonsingular orbital elements L, e_X, e_Y to resolve the numerical issue [17].

It is important to note that not all SV will be visible to all RS for time epoch k . To lighten the notations, these cases are not explicitly expressed in equation (13). But the corresponding rows must be removed whenever the measurements are unavailable. Equation (13) is simplified by respectively defining Z, H, N and ε as the measurement vector, observation matrix, state vector, and error vector.

$$Z_k = H_k N_k + \varepsilon_k \quad (14)$$

Dynamic model

$$\begin{bmatrix} \delta p^{orb} \\ \tau \\ b^{clk} \\ \eta \\ \varepsilon_{tropo}^{ZTD} \end{bmatrix}_{k+1} = \begin{bmatrix} \mathbf{I} & \mathbf{0} & \mathbf{0} & \mathbf{0} & \mathbf{0} \\ \mathbf{0} & \mathbf{I} & \mathbf{0} & \mathbf{0} & \mathbf{0} \\ \mathbf{0} & \mathbf{0} & \mathbf{I} & \mathbf{0} & \mathbf{0} \\ \mathbf{0} & \mathbf{0} & \mathbf{0} & \mathbf{I} & \mathbf{0} \\ \mathbf{0} & \mathbf{0} & \mathbf{0} & \mathbf{0} & e^{-T/\mu} \mathbf{I} \end{bmatrix} \begin{bmatrix} \delta p^{orb} \\ \tau \\ b^{clk} \\ \eta \\ \varepsilon_{tropo}^{ZTD} \end{bmatrix}_k + \begin{bmatrix} \mathbf{0} & \mathbf{0} & \mathbf{0} \\ \mathbf{1} & \mathbf{0} & \mathbf{0} \\ \mathbf{0} & \mathbf{1} & \mathbf{0} \\ \mathbf{0} & \mathbf{0} & \mathbf{0} \\ \mathbf{0} & \mathbf{0} & \mathbf{1} \end{bmatrix} \begin{bmatrix} \omega_{\tau}^{clk} \\ \omega_b^{clk} \\ \omega_{tropo}^{ZTD} \end{bmatrix} \quad (15)$$

$$N_{k+1} = \phi N_k + \Gamma \omega_k \quad (16)$$

The color-code for the terms highlighted in equation (15) is consistent with equation (13). But equation (15) is written in vector-form by stacking together the corresponding scalar quantities. The orbit parameters are constant throughout T_{FIT} . Since our goal is to estimate clocks instantaneously, infinite process noise is added to both SV and RS clock states. Thus, the estimator completely relies on the measurements for determining the clock states. Cycle ambiguities are constant but will be reset if cycle slip occurs. The ZTD residuals, in the last row, are treated as First Order Gauss Markov Processes where T is the sample period, μ is the time constant and the variance of ω_{tropo}^{ZTD} is $(1 - e^{-2T/\mu})\sigma_{ZTD}^2$ [22].

Using the equations (14) and (16), Information Filter can be implemented to estimate N . During the first few time-steps when running the filter, the estimated SV and RS clock biases would be poor. To get better estimates of the clock bias states, especially in these first few time steps, a backward information filter is run. The forward and backward filter together are referred to as the information smoother. The main advantages of this implementation are its time and memory-efficiency and the fact that no prior knowledge is used on any states except on the ZTD residual error.

The SV i 's orbit parameters δP_i^{orb} and clock bias $\tau_{i,k}$ can be extracted from the estimated state vector \hat{N}_k and the SV position is obtained by substituting the estimated orbit parameter into equation (2). Note that, estimated clock bias $\tau_{i,k}$ includes a relativistic correction also, but we mainly focus on satellite clock bias faults because of its drift. Thus, relativistic correction is computed using the estimated orbit parameter and removed from the estimated clock bias states.

V COVARIANCE ANALYSIS

In this section, a covariance analysis illustrates the contribution of measurement errors on σ_{OFM} . The information smoother provides an estimated state covariance matrix $\hat{\Sigma}_k$. To validate the ISM, we only need SV orbit parameters and clock information; the corresponding elements can be extracted from \hat{P}_k . For example, SV i 's orbit parameters and clock bias at time epoch k are extracted and arranged in a vector labeled $D_{i,k}$ with a dimension of 16×16 . Then, the 4×4 covariance matrix $\hat{P}_{LL,i,k}$ of the

satellite position and clock in the local-level (LL) reference frame (along-track, cross-track, radial) can be evaluated using the following equation:

$$\hat{P}_{LL,i,k} = \begin{bmatrix} R_{LL,i,k} & 0 \\ 0 & 1 \end{bmatrix} C_{i,k} D_{i,k} C_{i,k}^T \begin{bmatrix} R_{LL,i,k} & 0 \\ 0 & 1 \end{bmatrix}^T \quad (17)$$

where $R_{LL,i,k}$ is the ECEF to LL rotation matrix, and $C_{i,k}$ is defined as:

$$C_{i,k} = \begin{bmatrix} A_{i,k}^{orb} & 0 \\ 0 & 1 \end{bmatrix} \quad (18)$$

To investigate the SIS performance in the range domain, we evaluate the maximum Signal-In-Space Ranging Error (SISRE) standard deviation at the worst-case user location. This is achieved by projecting $\hat{P}_{LL,i,k}$ along line-of-sights for all locations within SV footprint [13]. And the worst-case SISRE standard deviation $\sigma_{SISRE,i,k}$ is defined as the maximum standard deviation over all of these locations. In Figure 4, the projection region is shaded in light blue, and the black dashed line is one example projection line $G_{i,m}$, where m is the index of the user location. Therefore, $\sigma_{SISRE,i,k}^2$ is given by:

$$\sigma_{SISRE,i,k}^2 = \max_{m=i,\dots,ALL} (G_{i,m} \hat{P}_{LL,i,k} G_{i,m}^T) \quad (19)$$

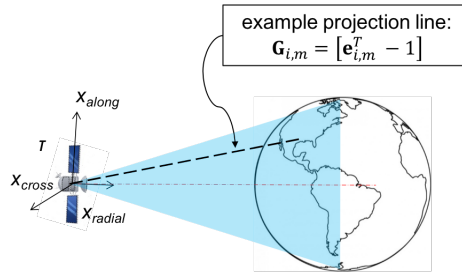


Fig. 4. Covariance matrix projection along LOS for all locations

VI ERROR MODEL

For the OFM prototype, we collected code and carrier measurements from 20 IGS stations (Figure 3). In prior work, we have characterized iono-free code RNM errors for each RS, which were overbounded by Gaussian distribution with zero mean and standard deviation of 1 m to 3 m depending on elevation angle [17]. For example, Table I shows RNM code errors for one of the IGS stations (station code - 'kokv'). Note that below 10-degree elevation, few measurements are available. Therefore, the prototype uses measurements above 10-degree elevation for all RS.

TABLE I
CODE ERROR MODEL FOR IGS RS 'KOKV'

Elevation (deg.)		Mean (m)	Bounded sigma (m)	No of samples
Min.	Max.			
0	10	0.29	4.11	35
10	15	0.07	2.79	1067
15	20	0.02	2.55	2250
20	25	0.07	1.88	3069
25	30	0.06	1.49	2338
30	35	0.01	1.22	2127
35	40	0.08	1.05	2231
40	90	0.06	1.06	10669

In prior work, we have shown the sensitivity of carrier phase RNM error on the estimator [17]. It is important to model this error properly, but currently, the prototype assumes a simple carrier error model. Table II shows the inclusion criteria

of measurements depending on carrier noise ratio (C/N_0) on L1 and L2 frequency. Since low C/N_0 carrier measurements are included from half of the stations to get the observability on H_k , we assume that raw L1 and L2 carrier phase noise can be overbounded by a Gaussian distribution with zero mean and standard deviation of 2 cm. Taking into account the noise inflation on the iono-free carrier noises (L1/L2), the standard deviation of carrier measurements in equation (13) becomes 5.96 cm.

TABLE II
INCLUSION CRITERIA FOR MEASUREMENTS

RS index	RS code	C/N_0		RS index	RS code	C/N_0	
		Min. on L1	Min. on L2			Min. on L1	Min. on L2
1	LCK4	35	34	11	NRIL	35	35
2	STK2	35	26	12	LAMA	35	35
3	CEDU	35	26	13	CASI	35	27
4	DAV1	35	35	14	SASK	35	27
5	DGAR	35	35	15	REUN	35	27
6	KOKV	35	26	16	PIEL	35	27
7	PALM	35	35	17	ZAMB	35	35
8	YKRO	35	35	18	LAUT	35	27
9	MAJU	35	27	19	ISPA	35	35
10	UFPR	0	0	20	LMMF	34	27

Also, we assumed that the tropo model (UNB3m [21]) was valid for all IGS RS and that the ZTD residual errors could be modeled using a First-order Gauss Markov Process with zero mean, a standard deviation of 5 cm and a time constant of 30 minutes [20].

VII NUMERICAL STABILITY OF THE ESTIMATOR

VII-A Computation of Jacobian matrix

We have observed that the Jacobian matrix in equation (9) is a critical element of the OFM. Here, we pursue a numerical approach to calculate partial derivative by choosing a small deviation in the parameters (Δp). Initially, we used Newton's difference quotient method to compute approximate derivative using two-points. Since SV position is a highly non-linear function of orbit parameters, higher-order errors exist in this method. Therefore, we use the following equation using four-point to compute the derivative [28].

$$\frac{df}{dp} = \frac{f(p - 2\Delta p) - 8f(p - \Delta p) + 8f(p + \Delta p) - f(p + 2\Delta p)}{12\Delta p} \quad (20)$$

Moreover, choosing an appropriate small deviation (Δp) is also crucial. If we choose a larger Δp , it produces inaccurate derivative. On the other hand, choosing too small a value introduces rounding errors. Instead, we utilize the Richardson extrapolation method to achieve precise derivatives [29]. In this method, we input a large Δp and a required precision limit (ϵ) on the derivative, which automatically adjusts Δp to converge to an actual derivative. The suitable input Δp for the GPS legacy model is validated and shown in Table III.

TABLE III
INPUT SMALL DEVIATION TO RICHARDSON EXTRAPOLATION METHOD

orbital parameter	M_0	Δn	e	\sqrt{A}	Ω	i_0	ω	$\dot{\Omega}$	IDOT	Cuc	Cus	Crc	Crs	Cic	Cis
Δp	10^{-2}	10^{-6}	10^{-5}	1	10^{-2}	10^{-2}	10^{-2}	10^{-6}	10^{-6}	10^{-2}	10^{-2}	1	1	10^{-2}	10^{-2}
ϵ	10^{-3}	100	1	10^{-1}	10^{-3}	10^{-3}	10^{-3}	1	1	1	1	10^{-7}	10^{-7}	1	1

VII-B Modification to observation matrix

Once we obtain the Jacobian matrix, one would see that nominal partial derivatives would lie between the order of 10^6 to 10^{11} . This large difference in magnitude of the derivatives creates an ill-conditioned observation matrix in equation (13). As we have implemented information filter, this causes numerical problems while inverting the information matrix. Due to ill-conditioned information matrix, estimated states are jittery rather than being constant. Figure 5 shows one of the estimated orbital parameters. To address this issue, we modify the observation matrix.

The current measurement model (13) is rewritten in the following equation for orbit parameter states δp and other states X_0 . Here, our goal is to balance the singular values of H_k by modifying B_k ; O_k is corresponding to other states which remain the same.

$$Z_k = \begin{bmatrix} B_k & O_k \end{bmatrix} \begin{bmatrix} \delta p \\ X_o \end{bmatrix}_k + \varepsilon_k \quad (21)$$

Instead of estimating deviation in orbital parameters, now the actual parameters are estimated.

$$Z_k + \begin{bmatrix} B_k & O_k \end{bmatrix} \begin{bmatrix} p^* \\ 0 \end{bmatrix} = \begin{bmatrix} B_k & O_k \end{bmatrix} \begin{bmatrix} p \\ X_o \end{bmatrix}_k + \varepsilon_k \quad (22)$$

The orbital parameter states are augmented such that new states are normalized to linearized parameters (p^*), which results in a better conditional number of the observation matrix. However, the elements of the observation matrix corresponding to $L, e_x, e_y, \sqrt{A}, \Omega, i_0$ orbital states still lie in the order of 10^6 . Therefore, those elements are divided by 10^6 to refine the conditional number of the observation matrix (this is not shown explicitly in equation (23)). The parameters which are zeros during the linearization are then replaced by 10^{-6} . An information smoother utilizes the modified measurement equation (23) and provides a more stable performance. Figure 6 shows the expected constant parameter compared to Figure 5.

Figure 6 shows the improved orbital state which is constant as we expected.

$$Z_k + \begin{bmatrix} B_k & O_k \end{bmatrix} \begin{bmatrix} p^* \\ 0 \end{bmatrix} + \begin{bmatrix} B_k & O_k \end{bmatrix} \begin{bmatrix} -p^* & 0 \\ 0 & 1 \end{bmatrix} \begin{bmatrix} 1 \\ 0 \end{bmatrix} = \begin{bmatrix} B_k & O_k \end{bmatrix} \begin{bmatrix} -p^* & 0 \\ 0 & 1 \end{bmatrix} \begin{bmatrix} 1 - \frac{p}{X_o} \\ p^* \end{bmatrix}_k + \varepsilon_k \quad (23)$$

$$Z_{new,k} = H_{new,k} \begin{bmatrix} 1 - \frac{p}{X_o} \\ p^* \end{bmatrix}_k + \varepsilon_k$$

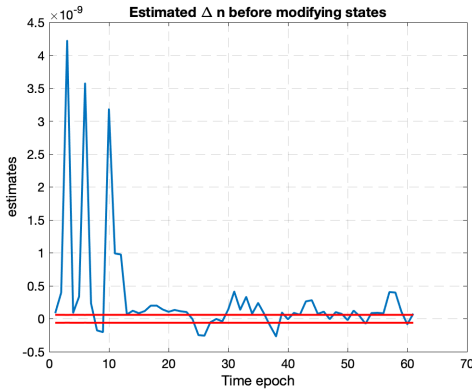


Fig. 5. Estimated orbital parameter before modification

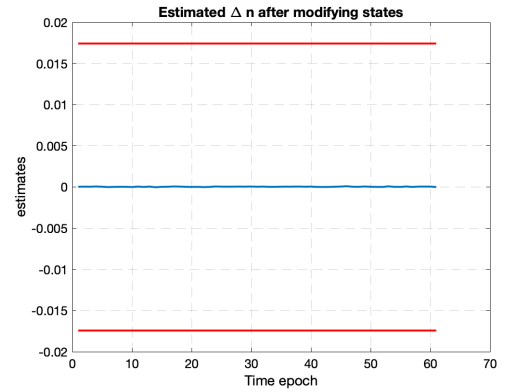


Fig. 6. Estimated orbital parameter after modification

VIII RESULTS

We use raw code and carrier measurements from 20 IGS station to evaluate satellite orbit and clocks. The reported RS locations are obtained from SINEX input file which is a data interchange format for precise antenna position [27]. To validate the prototype, we use ‘orbit product’ from the Jet Propulsion Laboratory (JPL), which provides SV orbit and clock biases with an accuracy of 2.5 cm. Moreover, this orbit and clock product is verified by comparing it to another analysis center named Natural Resources Canada (EMR) for a one-time epoch. For instance, the magnitude of SV orbit and clock bias errors are shown in Figure 7 for date 1-3-2016 on UTC 6:00. One important point is that these orbit positions are referenced to the satellite center of mass (COM), while the orbital model and measurements are valid to SV antenna phase center (APC). To compare these products with our estimated OFM results, we transform SV COM position to APC., where the relative distance from COM to APC is available from the Antenna Exchange Format (ANTEX) file and shown in Figure 8.

To run the proposed information smoother, data is collected over 4 hours period with a sample interval of 4 minutes, which essentially eliminates the time correlation of the measurement errors. The information smoother is executed using equations (23) and (15). As a result, we obtain the orbit parameters and the SV clock bias every 4 minutes (RS clock biases and cycle ambiguities are also obtained but are not needed for validating the ISM). To evaluate the OFM performance, measurements from

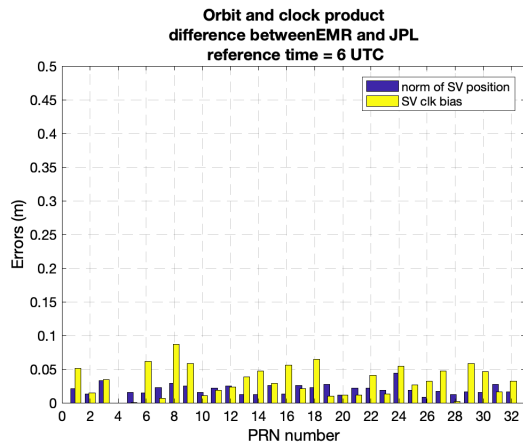


Fig. 7. Comparing JPL product with EMR product

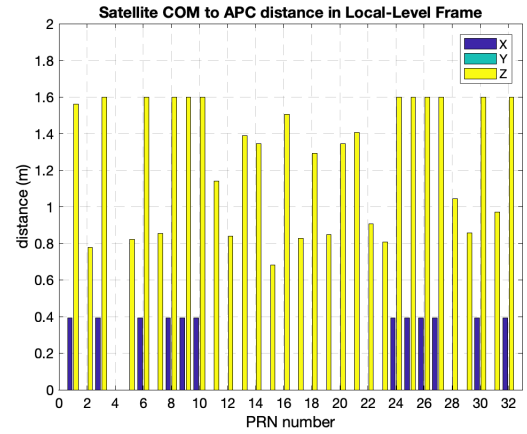


Fig. 8. Satellite COM to APC offset

UTC 4:00 to 8:00 on 1-3-2016 are fed into the information smoother. Figure 10 shows the standard deviation of SISRE using the estimated parameters. Since the standard deviation is below 0.4 m during the central two hours, the estimated parameters are considered for the central two hours (between 5:00 and 7:00). To make the comparison simpler, SV orbit and clock biases are extracted for UTC 6:00 and compared to the JPL product. The residual errors of OFM are obtained by equations (24) and (25). Finally, the resulting SISRE is evaluated using equation (27) as shown in Figure 9 [19].

$$r_i^{orb} = X_i^{JPL,APC} - g_k^{orb}(\hat{p}_i^{orb}) \quad (24)$$

$$r_{clock} = \tau_i^{JPL} - \hat{\tau}_i \quad (25)$$

Where, \hat{p}_i^{orb} is the estimated orbit parameter vector.

$$r_{LL,i} = R_{LL,i} r_i^{orb} = [r_{A,i} \quad r_{C,i} \quad r_{R,i}]^T \quad (26)$$

$$r_{SISRE} = (r_{R,i} + r_{clock}) + 0.24 \operatorname{sgn}(r_{R,i} + r_{clock}) \sqrt{r_{A,i}^2 + r_{C,i}^2} \quad (27)$$

Where,

$r_{R,i}$: the radial position component of the residual

$r_{A,i}$: the along-track position component

$r_{C,i}$: the cross-track position component

r_{clock} : the clock component (in unit length)

The majority of the estimated SISRE is close to the standard deviation. However, one may question the reliability and accuracy of the estimated product by observing Figures 9 and 10. There are mainly two reasons behind these larger errors. Firstly, some SV tracks do not have enough RS to ensure good observability. Figure 10 shows the event where PRN 2 has lost the observability after UTC 7. Secondly, we have utilized carrier phase measurements which have low C/N_0 (Table II). Those low C/N_0 measurements may have large carrier noise. This is why it is essential to characterize the carrier phase error at low C/N_0 . So once we accurately characterize the errors from low C/N_0 measurements, it is expected to lower the SISRE.

IX CONCLUSION

This paper describes a prototype to estimate satellite orbit and clock biases for ARAIM OFM, which aims at validating the ISM for ARAIM users. The prototype employs a worldwide network of sparsely-distributed reference stations (RS) and a parametric orbit model to simultaneously estimate SV orbit parameters, SV clock biases, and RS clock biases. An information smoother is implemented for time and memory efficiency. Furthermore, we have resolved numerical issues resulting from the Jacobian matrix sensitivity and ill-conditioned observation matrices. The stability of the estimator has been improved, and estimated “truth” product has a standard deviation of 0.4 m and maximum SISRE of 1.2 m. In the future, we will characterize the low C/N_0 carrier phase measurement error to utilize more measurements, and the time-correlation of code and carrier errors

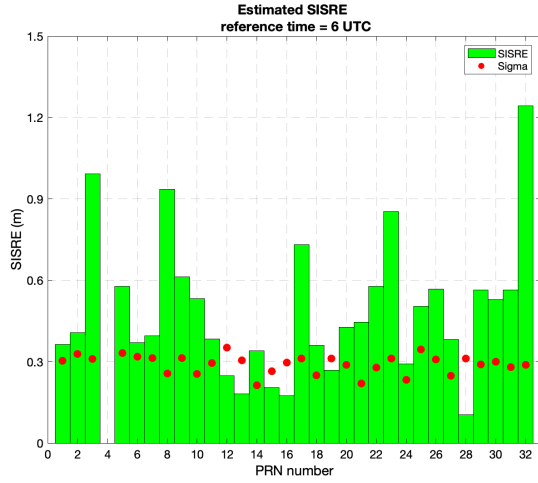


Fig. 9. Comparing estimated SV position and clock bias with JPL product while using legacy model

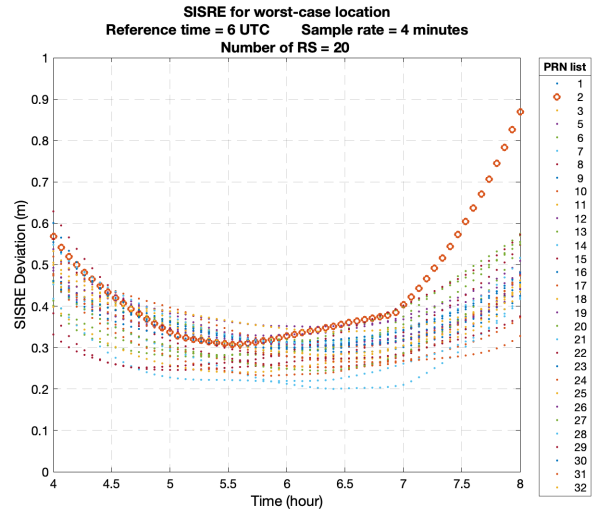


Fig. 10. SISRE deviation on the estimated orbit and clock using legacy model

will be modeled to run estimator at higher sampling rates. Further, we will implement the CNAV orbit model to improve orbit determination performance.

ACKNOWLEDGMENT

The authors would like to thank the Federal Aviation Administration (FAA) for their continued support of this research effort. The opinions in this paper are our own and do not represent those of the FAA, any other person or organization.

Appendix A

DIFFERENTIAL CODE BIAS (DCB)

The code phase measurement type for SV i from RS j is expressed as:

$$\rho_w^{i,j} = \|X_j - X_i\| - \tau_{i,k} + b_{j,k} + c(d_j + d_w^i) + T^{i,j} + I^{i,j} + \varepsilon_{RNM,\rho,k}^{i,j} \quad (28)$$

where,

w : represents types of received code. i.e. C/A, P(Y) or C/A using cross-correlation

$I^{i,j}$: Ionospheric delay errors for SV i and RS j

Now, the GPS constellation time is defined by iono-free combination using P1 and P2 code measurements.

$$\begin{aligned} \rho_{IF}^{i,j} &= \frac{f_{L1}^2}{f_{L1}^2 - f_{L2}^2} \rho_{P1} - \frac{f_{L2}^2}{f_{L1}^2 - f_{L2}^2} \rho_{P2} \\ &= r^{i,j} + T + c(\delta t_j - \delta t^i) + c \underbrace{\left(\frac{f_{L1}^2}{f_{L1}^2 - f_{L2}^2} d_{P1}^i - \frac{f_{L2}^2}{f_{L1}^2 - f_{L2}^2} d_{P2}^i \right)}_{=0} + \varepsilon_{\rho_{IF}} \end{aligned} \quad (29)$$

Where,

$\left(\frac{f_{L1}^2}{f_{L1}^2 - f_{L2}^2} d_{P1}^i - \frac{f_{L2}^2}{f_{L1}^2 - f_{L2}^2} d_{P2}^i \right)$ is considered as a zero and instrumental delays are observed with respect to d_{P1}^i and d_{P2}^i

The iono-free measurement is expressed for L1 code type $w1$ and L2 code type $w2$:

$$\begin{aligned}
\rho_{IF}^{i,j} &= \frac{f_{L1}^2}{f_{L1}^2 - f_{L2}^2} \rho_{w1} - \frac{f_{L2}^2}{f_{L1}^2 - f_{L2}^2} \rho_{w2} \\
&= r^{i,j} + T + c(\delta t_j - \delta t^i) + c \left(\frac{f_{L1}^2}{f_{L1}^2 - f_{L2}^2} d_{w1}^i - \frac{f_{L2}^2}{f_{L1}^2 - f_{L2}^2} d_{w2}^i \right) + \varepsilon_{\rho_{IF}} \\
&= r^{i,j} + T + c(\delta t_j - \delta t^i) + c \left(\frac{f_{L1}^2}{f_{L1}^2 - f_{L2}^2} (d_{P1}^i + d_{w1}^i - d_{P1}^i) - \frac{f_{L2}^2}{f_{L1}^2 - f_{L2}^2} (d_{P2}^i + d_{w2}^i - d_{P2}^i) \right) + \varepsilon_{\rho_{IF}} \\
&= r^{i,j} + T + c(\delta t_j - \delta t^i) c(\delta t_j - \delta t^i) + c \underbrace{\left(\frac{f_{L1}^2}{f_{L1}^2 - f_{L2}^2} d_{P1}^i - \frac{f_{L2}^2}{f_{L1}^2 - f_{L2}^2} d_{P2}^i \right)}_{=0} \\
&\quad + c \left(\frac{f_{L1}^2}{f_{L1}^2 - f_{L2}^2} (d_{w1}^i - d_{P1}^i) - \frac{f_{L2}^2}{f_{L1}^2 - f_{L2}^2} (d_{w2}^i - d_{P2}^i) \right) + \varepsilon_{\rho_{IF}} \\
&= r^{i,j} + T + c(\delta t_j - \delta t^i) + c \left(\frac{f_{L1}^2}{f_{L1}^2 - f_{L2}^2} DCB_{w1-P1}^i - \frac{f_{L2}^2}{f_{L1}^2 - f_{L2}^2} DCB_{w2-P2}^i \right) + \varepsilon_{\rho_{IF}}
\end{aligned} \tag{30}$$

Since the prototype uses C1 type of L1 code and P2 type of L2 code measurement, we only need DCB_{C1-P1} for all the SV. Depending on the types of code and frequency, DCB correction can be applied as shown in the above equation. Currently, DCB product is obtained from IGS [26] and maybe reproduce as shown in [25].

Appendix B SOLID EARTH TIDE

Solid Earth tide is the displacement of the solid earth's surface caused by the gravity of the Moon and Sun. It can be modeled by a spherical harmonics expansion and associated physical parameters known as Love and Shida Numbers., which describes the susceptibility of the Earth's body to the tide-generating potential [30]. The solid earth tide correction mainly depends on the latitude of antenna location and varies between 5 cm to 10 cm over a day. For example, this correction is shown for one of the used RS in Figure 11.

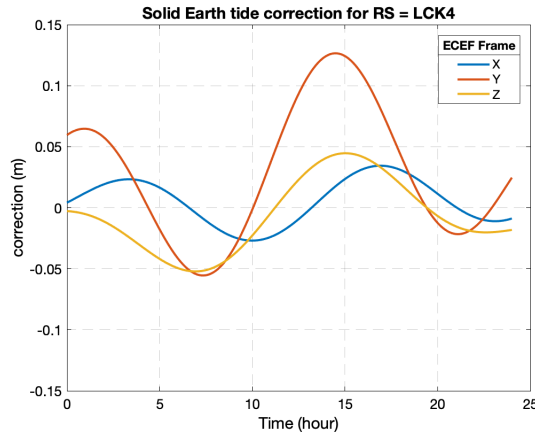


Fig. 11. Solid Earth tide correction

References

- [1] Pervan, B., "Navigation integrity for aircraft precision landing using the global positioning system," Ph.D. Dissertation, Dept. of Aeronautics and Astronautics, Stanford Univ., Stanford, CA, 1996.
- [2] Lee, Y. C., "Analysis of Range and Position Comparison Methods as a Means to Provide GPS Integrity in the User Receiver," Proceedings of the 42nd Annual Meeting of The Institute of Navigation, Seattle, WA, 1986, pp. 1-4.

- [3] Parkinson, B. W., and Axelrad, P., "Autonomous GPS Integrity Monitoring Using the Pseudorange Residual," *NAVIGATION: Journal of the Institute of Navigation*, Vol. 35, No. 2, 1988, pp. 255–274. doi:10.1002/j.2161-4296.1988.tb00955.x
- [4] RTCA Special Committee 159, "Minimum Operational Performance Standards for Airborne Supplemental Navigation Equipment Using Global Positioning System (GPS)," RTCA/DO-208, July 1991.
- [5] Joerger, M., Chan, F.-C., and Pervan, B., "Solution Separation Versus Residual-Based RAIM," *NAVIGATION: Journal of the Institute of Navigation*, Vol. 61, No. 4, Winter 2014, pp. 273-291. doi: 10.1002/navi.71
- [6] Gibbons, G., "Munich Summit Charts Progress of GPS, GLONASS, Galileo, Beidou GNSSes," *Inside GNSS*, March 20, 2012.
- [7] EU-US Cooperation on Satellite Navigation, WG CARAIM Technical Subgroup, "ARAIM Technical Subgroup Interim Report, Issue 1.0", 2012.
URL: <http://www.gps.gov/policy/cooperation/europe/2013>
- [8] EU-U.S. Cooperation on Satellite Navigation, Working Group C, "ARAIM Technical Subgroup Milestone 2 Report," February 11, 2015.
URL: <http://www.gps.gov/policy/cooperation/europe/2015/working-group-c/>
- [9] Blanch, J., T. Walter, P. Enge, S. Wallner, F. A. Fernandez, R. Dellago, R. Ioannides, I. F. Hernandez, B. Belabbas, A. Spletter, M. Rippl, "Critical Elements for a Multi-Constellation Advanced RAIM," *NAVIGATION*, Vol. 60, No. 1, 2013, pp. 53-69.
- [10] Blanch, J., Walter, T., Enge, P., Lee, Y., Pervan, B., Rippl, M., Spletter, A., and Kropp, V., "Baseline Advanced RAIM User Algorithm and Possible Improvements," *IEEE Transactions on Aerospace and Electronic Systems*, Vol 51, January 2015, pp. 713- 732.
doi: 10.1109/TAES.2014.130739
- [11] Phase II of the GNSS Evolutionary Architecture Study, February 2010.
URL: https://www.faa.gov/about/office_org/headquarters_offices/ato/service_units/techops/navservices/gnss/library/documents/media/G_EASPhaseII_Final.pdf
- [12] Blanch, J., et al, "Architectures for Advanced RAIM: Offline and Online," *Proceedings of the 27th International Technical Meeting of The Satellite Division of the Institute of Navigation (ION GNSS+ 2014)*, Tampa, Florida, September 2014, pp. 787-804.
- [13] Walter, T., Blanch, J., "Keynote: Characterization of GNSS Clock and Ephemeris Errors to Support RAIM," *Proceedings of the ION 2015 Pacific PNT Meeting*, Honolulu, Hawaii, April 2015, pp. 920-931.
- [14] Perea, S., Meurer, M., Rippl, M., Belabbas, B., and Joerger, M., "URA/SISA Analysis for GPS and Galileo to Support RAIM," *NAVIGATION: Journal of the Institute of Navigation*, Vol. 64, No. 2, Summer 2017, pp. 237-254. doi: 10.1002/navi.199.
- [15] Walter, T., Gunning, K., Blanch, J., "Keynote: Validation of the Unfaulted Error Bounds for RAIM," *Proceedings of the ION 2017 Pacific PNT Meeting*, Honolulu, Hawaii, May 2017, pp. 1-19.
- [16] Zhai, Y., Joerger, M., Pervan, B., "A Dedicated RAIM Ground Monitor to Validate the Integrity Support Message," *Proceedings of Institute of Navigation GNSS+ 2017 Conference*, Portland, OR, Sep 2017, pp. 1063-1076.
- [17] Patel, J., Zhai, Y., Kiarash, S., Khanafseh, S., Joerger, M., Pervan, B., "Prototyping an RAIM Offline Ground Monitor Using Experimental Data," *Proceedings of Institute of Navigation GNSS+ Conference*, Miami, FL, Sep 2018, pp. 2583-2597.
- [18] Global Positioning System Directorate Systems Engineering and Integration, "Interface Specification IS-GPS-200," Revision H, 2013.
<http://www.gps.gov/technical/icwg/IS-GPS-200H.pdf>
- [19] Joerger, M., Zhai, Y., Pervan, B., "Online Monitor Against Clock and Orbit Ephemeris Faults in RAIM," *Proceedings of the ION 2015 Pacific PNT Meeting*, Honolulu, Hawaii, April 2015, pp. 932-945.
- [20] RTCA Special Committee 159. (2006). *Minimum Operational Performance Standards for Global Positioning System/Wide Area Augmentation System Airborne Equipment*. RTCA/DO-229D.
- [21] Leandro R.F., M.C. Santos, and R.B. Langley (2006). *UNB Neutral Atmosphere Models: Development and Performance*. *Proceedings of ION NTM 2006*, the 2006 National Technical Meeting of The Institute of Navigation, Monterey, California, 18-20 January 2006; pp. 564-573.
- [22] Gelb, A., "Applied Optimal Estimation," the MIT Press, 2001.
ISBN: 0-262-57048-3
- [23] AIAA, Education Series, J.S. Przemieniecki/series editor-in-chief.
An introduction to the Mathematics and Methods of Astrodynamics, Revised Edition. Richard H. Battin
- [24] J. Rife, S. Pullen, P. Enge, and B. Pervan, "Paired Overbounding for Nonideal LAAS and WAAS Error Distributions," *IEEE Transactions on Aerospace and Electronic Systems*, Vol. 42, No. 4, October 2006, pp. 1386-1395.
- [25] Wang, N., Yuan, Y., Li, Z., Montenbruck, O., Tan, B., "Determination of differential code biases with multi-GNSS observations" *Journal of Geodesy*, Vol 90, Issue 3, March 2016, pp 209–228.
<https://doi.org/10.1007/s00190-015-0867-4>
- [26] Source of differential code bias for satellite.
https://cddis.nasa.gov/Data_and_Derived_Products/GNSS/gnss_differential_code_bias_product.html
- [27] Source of Precise antenna position for IGS reference station.
https://cddis.nasa.gov/Data_and_Derived_Products/GNSS/station_position_products.html
- [28] *Fundamental Numerical Methods and Data Analysis* by George W. Collins, II
- [29] Richardson, L. F. (1911). "The approximate arithmetical solution by finite differences of physical problems including differential equations, with an application to the stresses in a masonry dam". *Philosophical Transactions of the Royal Society A*. 210 (459–470): 307–357.
doi:10.1098/rsta.1911.0009
- [30] Petit, G., Luzum, B., : *IERS Conventions (2010)*, IERS Technical Note No. 36, Frankfurt 2010